Article

Removal of Eutrophication Agents from Wastewater Using Glauconite-Based Sorbents

Kateryna Stepova[1], Iryna Fediv[2]*, Aušra Mažeikienė[3], Vasyl Kordan[4] and Dainius Paliulis[5]

[1] Department of Environmental Safety, Lviv State University of Life Safety, 35 Kleparivska str., 79000, Lviv, Ukraine, katyastepova@gmail.com;

[2] Department of Environmental Safety, Lviv State University of Life Safety, 35 Kleparivska str., 79000, Lviv, Ukraine, ira.arnaut94@gmail.com;

[3] Department of Environmental Protection and Water Engineering, Faculty of Environmental Engineering, Vilnius Gediminas Technical University, Vilnius, Lithuania. Saulėtekio al. 11, LT-10223 Vilnius, Lithuania; email: ausra.mazeikiene@vilniustech.lt;

[4] Department of Inorganic Chemistry, Ivan Franko National University of Lviv, Kyryla i Mefodiya St. 6, 79005, Lviv, Ukraine; email: vasyl.kordan@lnu.edu.ua;

[5] Department of Environmental Protection and Water Engineering, Faculty of Environmental Engineering, Vilnius Gediminas Technical University, Vilnius, Lithuania. Saulėtekio al. 11, LT-10223 Vilnius, Lithuania; email: dainius.paliulis@vilniustech.lt;

* Correspondence: ira.arnaut94@gmail.com

Abstract: Excessive phosphorus and nitrogen in water and sediment may cause eutrophication, which poses a potential risk to drinking water safety and the sustainability of aquatic ecosystems. The research focuses on the removal of phosphates and ammonium ions from aqueous solutions using a new thermally and microwave-treated glauconite. The surface morphology of the samples was studied by SEM. BET surface area, pore volume, and pore size distribution were measured. Adsorption studies were carried out in static and dynamic conditions. The best fit for adsorption of the both pollutants is given by Langmuir-Freundlich and BET models. The calcined sample showed the lowest adsorption capacity for phosphate but the highest capacity for ammonium. Conversely, for the microwave-irradiated sample, the adsorption capacity for phosphate increases, while that for ammonium remains at the same level. In dynamic conditions phosphorus was most efficiently retained by natural glauconite, and ammonium nitrogen by glauconite that was thermally treated in a muffle furnace.

Keywords: glauconite; adsorption; eutrophication agents; water pollution; thermal treatment; microwave irradiation.

1. Introduction

Water pollution is one of the main environmental issues that has released contaminating substances into fresh water bodies or groundwater [1]. Natural water sources are polluted by untreated or insufficiently treated wastewater [2]. Variety of methods and technologies is developed for wastewater treatment. Usually, wastewater is treated using activated sludge microorganisms or chemical reagents. Conventional methods effectively remove organic matter from wastewater, but it is not possible to remove phosphorus completely [3]. Nitrogen is another threatening biogenic element that escapes into the environment with wastewater [4]. In recent years, there has been a significant focus on the advancement of new technologies for environmental protection (5-8). Excessive P and N in water and sediment can cause eutrophication, which poses a potential risk to drinking water safety and the sustainability of aquatic ecosystems [5]. Effective removal of phosphorus and nitrogen from wastewater is therefore a key strategy to control eutrophication. The

final stage of technological processes should be additional treatment with sorbent materials [9]. Adsorption technology is the most widely used technology for wastewater treatment [6, 10-13]. The simplicity of design, speed, efficiency, and profitability determine the wide use of sorbents [14]. Commercially available sorbents are rather expensive, which significantly limits the range of their application areas [15]. In this context, natural clay mineral adsorbents can be used as an alternative [14]. Natural adsorbents are inexpensive, environmentally friendly, and available in large quantities [7, 13]. Natural silicates possessing high adsorption, ion exchange, molecular-sieve, and catalytic characteristics deserve special attention [15-18]. Often, nitrogen in wastewater is in the ammonium form, so it can be removed by ion exchange. Ammonium ions are effectively removed from water or wastewater by zeolites [19, 20]. Most clay minerals produce a net negative surface charge due to the isomorphic substitutions of Si (IV) by Al (III) or Fe (III) [1]. Iron-based materials exhibit high efficiency for P immobilization due to their strong affinity with P [5]. The Fe-rich sorbents can effectively immobilize P in sediment under oxic conditions through adsorption and/or precipitation [8, 21]. However, not all natural clays are suitable for wastewater treatment. Bauxite and olivine are not applicable due to the presence of significant amounts of lead and/or nickel [22]. For wastewater treatment, the big interest is represented by natural sorbents which concern glauconite. It can primarily be used as a long-term organic fertilizer because the potassium, iron, and phosphorus present in glauconite pass into the soil and improve its properties [23]. High efficiency glauconite is demonstrated at the clarification of water from salts of heavy metals, some organic and inorganic structures, and radionuclides [18, 24]. Galangashi et al. used glauconite to remove ammonium ions from water and found that ion exchange was the main mechanism for ammonium removal [25]. The efficiency of sorption in the mineral rock of various deposits is determined to a large extent by the content of granular glauconite in it, as well as by the presence of iron oxide in the composition [15]. The advantages of this mineral are as follows: wide circulation, cheapness, availability, granular structure, thermal stability, good ion exchange, and filtration properties [5]. Due to these properties, glauconite can be applied to environmental

technologies [26, 27]. Glauconite is a natural alumosilicate, dioctahedral micaceous phyllosilicate mineral. It is an aqueous aluminosilicate of iron, silica, and potassium oxide of unstable composition. The final composition can vary depending on the origin of the mineral and affect its sorption properties [5, 15]. Clay minerals are considered the most effective adsorbents, but the modification methods can improve the capacity, capability, and selectivity of the adsorption properties of clays [1]. Modification processes such as acid activation, heat treatment, column, organic functionalization are used to obtain the desired properties [28-30]. Microwave irradiation has proven successful in preparing new promising materials for water treatment by causing structural and textural changes that enhance the products' adsorption capacity [9, 31]. Sorptive capacity is an important parameter that allows evaluation of the durability of the sorbent material. It is determined during mixing tests. However, a unified methodology for determining the sorption capacity of aggregates has not yet been developed. For this reason, researchers obtain different values of the sorption capacity of the same aggregates. On the other hand, only a few studies have been focused on real wastewater treatment.

This research focuses on the removal of phosphates and ammonium ions from aqueous solutions using a new thermally and microwave-treated glauconite. A new method of glauconite modification was proposed, samples modified in several ways were produced and tested, and their properties were compared with the properties of natural glauconite. This work aimed to identify the physicochemical characteristics of Ukrainian glauconite and assess its sorption properties for extracting ammonium ions and phosphates from wastewater.

2. Materials and methods

2.1. Characterization of adsorbents

According to the related literature [32-34], heat treatment of sorbents can harden the structure and increase their sorption capacity. The initial sample of glauconite (pH of aqueous extract – 8.6; bulk density – 1049,85 kg/m3) was sieved to obtain a particle size fraction of 0.8-1.2

mm. To improve the performance characteristics of glauconite, it was pre-treated with the following methods: calcination at 550 °C for 3 hours, and microwave treatment for 30 min at 790 W.

2.1.1. SEM and EDS

The surface morphology of the powdered samples was studied by scanning electron microscopy (SEM). The qualitative and quantitative composition of the samples was determined using energy dispersive X-ray spectroscopy (EDS) on a Tescan Vega3 LMU electron microscope equipped with the advanced Oxford Instruments Aztec ONE system (CCD Si drift detector X-MaxN20). Before the study, the sample powders were applied to an electrically conductive film. The experiments were performed at a W-cathode voltage of 20-25 kV. The SE detector characterizes the surface morphology and details its irregularities, while the BSE detector shows the contrast of phases with different element fillings.

2.1.2. BET surface area and pore size distribution

Before starting the measurement, the samples were placed in a vacuum and degassed at 150 °C for 3 hours. BET surface area, pore volume, and pore size distribution of the studied sorbents, as well as nitrogen adsorption/desorption isotherms, were recorded by Quantachrome Autosorb-iQ-KR/MP automated, high-vacuum, gas sorption analyser. Measurements of nitrogen adsorption and desorption isotherms were conducted at -196 °C (77 K). The specific surface area was calculated by the BET (Brunauer–Emmett–Teller) equation. The density functional theory (DFT) and QSDFT method were applied for making the pore size distribution plot. The total pore volume was determined from the adsorption isotherm by measuring the amount of nitrogen adsorbed at a relative pressure of p/p0 = 0.99. All calculations were performed using the ASiQwin program (Version 2.0), developed by Quantachrome Instrument.

2.2. Experiments methodology

2.2.1. Adsorption isotherms

The sorption properties of the samples were investigated under static conditions. Batch experiments were conducted at room temperature for a 24-hour period.

Anhydrous salts KH_2PO_4 and NH_4Cl were used for preparing the model PO_4^{3-} and NH_4^+ solutions respectively. The working solutions were prepared from the initial solutions by repeated dilution with distilled water. The PO_4^{3-} concentration was determined by KFK-2 photoelectric colorimeter. For the measurement of NH_4^+ content, the Ionometer AI-125 was used.

The experimental results were fitted to the following three isotherm models:

- the Langmuir-Freundlich isotherm model [35]:

$$q_e = \frac{q_m (K_{LF} C_e)^{n_{LF}}}{1+(K_{LF} C_e)^{n_{LF}}} , \quad (1)$$

where q_e and C_e are and the equilibrium concentration in solid and liquid phases, respectively. q_m is the adsorption capacity. K_{LF} is the affinity constant, and n_{LF} is the coefficient of heterogeneity or a measure of the adsorption intensity.

- the Dubinin-Radushkevich model [36] :

$$q_e = q_m exp^{-Be^2} , \quad (2)$$

where B is the model's constant, and e – Polanyi potential.

- the BET model [37]:

$$q_e = \frac{q_m C_{BET} C_e}{(C_e - C_S)\left[1+(C_{BET}-1)\frac{C_e}{C_S}\right]} , \quad (3)$$

where C_{BET} is and constant of the model, and C_S is f concentration of solute at the moment of saturation of all layers.

148 The nonlinear modelling was carried out according to procedure described in our previous
149 works [38].

150 *2.2.2. Breakthrough curves*

151 Domestic wastewater (which had already been biologically treated in an individual plant)
152 was filtered on a laboratory bench (Fig. 1):

153

154 **Figure 1.** Laboratory bench with three columns

155

156 The wastewater was filtered (filtration rate 5 ml/min) through three columns, which were
157 filled as follows:

158 Column 1: supporting layer of pebbles; 7 cm high layer of quartz sand; mixed filler ("4"
159 glauconite (Glauconite for 3 hours in a muffle furnace at a temperature of 550 °C) plus 60 g of
160 quartz sand), 20 g of quartz sand.

161 Column 2: supporting layer of pebbles; 7 cm high layer of quartz sand; mixed filler ("3"
162 glauconite (Natural glauconite) plus 60 g of quartz sand), 20 g of quartz sand.

163 Column 3: supporting layer of pebbles; 7 cm high layer of quartz sand; mixed filler ("5"
164 glauconite (Glauconite 30 min under the influence of microwaves) plus 60 g of quartz sand), 20 g
165 of quartz sand.

166 The filtration experiment lasted 4 hours. Filtrate samples were taken hourly for ammonium
167 nitrogen and phosphate phosphorus concentration.

168 The initial concentration of PO_4-P in the wastewater was 4.85 mg/L; and the initial con-
169 centration of NH4-N was 16.1 mg/l.

170 The effectiveness of removing PO_4-P from wastewater was calculated according to for-
171 mula (4):

172 $$E_i = \frac{(C_{1i} - C_{2i})}{C_{1i}} \cdot 100, \quad (4)$$

where: E_i – effectiveness of removing PO_4-P, %; C1,i – concentration of PO_4-P before treatment, mg/L; $C_{2,i}$ – concentration of PO_4-P after treatment, mg/L. The study was repeated two more times to present the mean results of three experiments.

MERCK Spectroquant® tests were used to determine the phosphorus concentration of phosphates. Test limits 0.50-30.0 mg/l PO_4-P. Absorbance measurements of the test solution were performed by pouring test samples into 10 mm cuvettes (Hellma) and measuring at the required wavelength (410 nm) with a Genesys 10 UV–Vis spectrophotometer (Thermo Fisher Scientific, USA). MERCK Spectroquant® tests were used to determine ammonium nitrogen concentration. Test limits 2.0-75.0 mg/l NH_4-N. Absorbance measurements of the test solution were performed after 15 minutes by pouring test samples into 10 mm cuvettes (Hellma) and measuring at the required wavelength (690 nm) with a Genesys 10 UV–Vis spectrophotometer (Thermo Fisher Scientific, USA).

3. Results and discussion

3.1. SEM and EDS

Figure 2. SEM images of glauconite (SE detector on the left, BSE detector on the right): a - initial sample, b - calcined at 550 °C, c - microwave irradiated

Fig.2 shows the surface morphology of powdered samples of natural glauconite. The size of the crystallites of the original sample is 2-20 microns. The shape of the grains is similar to blocks with cut edges. The peculiarity of the stacking of these blocks is significant aggregation between them, probably due to crystallization water.

Heat or microwave treatment changes both the grain shape and morphology of the sample. Large aggregates of ~20 μm crack into smaller fragments (5-10 μm) with a highly developed surface during processing. In the case of thermal treatment, spherical particles can be observed

next to the blocky grains. On the surface of each particle, we can see microcracks, which contribute to further amorphization of the sample as the processing time increases. A similar effect is observed for the sample after microwave treatment. The evaporation of crystallization water causes the formation of micropores and microcracks and increases the surface area of the grains for further sorption of ammonium (NH_4^+) and phosphate (PO_4^{3-}) ions.

The overall composition of the sample does not undergo significant changes, as water is mainly released during the treatment. Some changes are due to the heterogeneity of the composition of natural glauconite. Fig. 3 shows the elemental distribution on the sample surface. The ratio of cations for the original sample is Na/Mg/Al/Si/K/Ca/Ti/Fe 1.17/1.07/13.39/74.41/4.45/4.00/0.35/1.16. The elemental ratios for the muffle furnace-annealed and microwave-irradiated samples are Mg/Al/Si/K/Ca/Fe 5.20/11.35/59.90/7.82/3.30/12.43 and Mg/Al/Si/K/Ca/Fe 5.76/11.52/58.36/7.42/4.09/12.85, respectively.

Figure 3. Elemental distribution on the surface of glauconite
a - initial sample, b - calcined at 550 °C, c - microwave irradiated

3.2. Surface area and porosity

The N_2 adsorption-desorption isotherms for natural and modified samples are presented in Fig.4. Due to hysteresis loops present on the plot of the samples we assume that the materials are mesoporous. The hysteresis loops in all the isotherms are of type IV (IUPAC) with the loops of the H3 type [39]. The H3 type is characterized by the presence of wedge-shaped pores, resulting from the loose arrangement of flaky particles. It is evident on the micrographs of the test samples (Fig. 4).

Figure 4. N_2 adsorption-desorption isotherms

The results of porosimetry are presented in Table 1. The equivalent particle size (d_{part}) was estimated using the relation (5) [40]:

$$d_{part} = \frac{6000}{S_{BET} \cdot \rho}, (5)$$

Where ρ is the density of bulk composite in g/cm^3 and S_{BET} is expressed in m^2/g. The porosity of the particles (ε) is calculated using the following equation (6) [41]:

$$\varepsilon = \frac{V_p}{V_p + {}^1/_{\rho_{app}}}, (6)$$

Where Vp is the pore volume (cm^3/g) and ρ_{app} is the apparent density (g/cm^3) of investigated materials.

It was found that high-temperature treatment reduces the BET surface area from 54.99 to 43.57 m^2/g. In contrast, under the influence of microwave irradiation, the surface area changes much less. However, an interesting fact was the increase in the external surface area of the glauconite sample under the influence of microwave irradiation with a simultaneous decrease in the micropore area. Whereas calcination at 550 °C causes only a decrease in the micropore surface area (Fig. 5). Expectedly, the equivalent particle size increases under the influence of high temperature due to sintering from 103.9 to 156.7 nm.

Table 1. Specific surface area (S_{BET}), micropore area (S_{mic}), external surface area (S_{ext}), pore volume (V_p), equivalent particle size (d_{part}), and porosity (ε) of natural and modified clinoptilolite.

Figure 5. Pore size distribution

3.2. Adsorption isotherms

The results of the nonlinear fitting of experimental research within theoretical models are presented in Tables 2 and 3.

Table 2. NH_4^+ adsorption isotherms nonlinear fitting parameters.

Table 3. PO_4^{3-} adsorption isotherms nonlinear fitting parameters.

The best fit for adsorption of the both pollutants is given by Langmuir-Freundlich model, but it doesn't provide any information about the adsorption mechanism. In order to identify the physical or chemical mechanism of adsorption the Dubinin-Radushkevich isotherm was used. From the determination of the average free energy of adsorption (E), the nature of the process can be inferred. The calculated values of E in all studied cases are less than 8 kJ/mol, so the adsorption process is of physical nature. Meanwhile the BET model also fits well to experimental data. This model describes the physical adsorption process rather well and allows the formation of n layers. The adsorption isotherms of NH_4^+ and PO_4^{3-} on natural and modified clinoptilolite are presented in Fig. 6 and 7 respectively.

Figure 6. Isotherms of NH_4^+ adsorption

Figure 7. Isotherms of PO_4^{3-} adsorption

The shapes of the curves are quite different. The isotherm of NH_4^+ adsorption corresponds to Type-IV according to the IUPAC classification [46], while the PO_4^{3-} isotherm corresponds to the Type-V. According to [42], Type-V isotherms are related to microporous materials, as opposed to the Type-VI isotherm where multilayer adsorption occurs on a uniform non-porous surface [43]. Therefore, it can be assumed that NH_4^+ is absorbed by the external surface of the samples, but phosphate ion is well fixed in the micropores. This coincides with the results of the porosity study

of the samples before and after treatment. As shown in Table 1, heat treatment at high temperatures leads to a significant decrease in microporosity by 42.3%. Therefore, it is the calcined sample that shows the lowest adsorption capacity for phosphate. In contrast, this increases the adsorption capacity of the sample for ammonium. Conversely, for the microwave-irradiated sample, the adsorption capacity for phosphate increases, while that for ammonium remains at the same level.

3.3. Breakthrough capacity

Fig. 8 clearly demonstrates that, in the initial two hours, both the natural and microwave-irradiated samples exhibited superior effectiveness of PO_4^{3-} removal compared to the thermally treated sorbent. 3 hours later, all three samples reached almost the same retention rate. The best result in terms of phosphate uptake was shown by the natural glauconite and slightly worse by the microwave irradiated sample. Thermal modification significantly worsens the sorption properties of glauconite for phosphate. Thus, in the case of phosphate absorption under dynamic conditions, heat treatment of glauconite does not lead to a significant improvement in sorption properties.

Figure 8. PO_4-P retention efficiency

A completely opposite phenomenon is observed in the ammonium absorption. As can be seen from Fig. 9, the highest removal rate during the first hour is demonstrated by the natural and heat-treated samples. However, subsequently, the ammonium retention efficiency begins to decrease sharply for both the natural and microwave irradiated samples. At the same time, the heat-treated sorbent continues effectively purifying water (more than 80% efficiency) even after 3 hours of exposure. Thus, in the case of ammonium nitrogen purification, heat treatment of glauconite significantly improves its sorption capacity.

Figure 9. NH_4-N retention efficiency

Hence, phosphate phosphorus and ammonium nitrogen retention took place in all columns. Phosphorus was most efficiently retained by natural glauconite, and ammonium nitrogen by glauconite that was calcinated in a muffle furnace for 3 hours at 550 °C. In general, all three columns removed ammonium nitrogen more efficiently than phosphate phosphorus.

4. Conclusions

New thermally and microwave-treated glauconite for removal of eutrophication agents (phosphate phosphorus and ammonium nitrogen) from aqueous solutions was investigated.

SEM-EDS investigation revealed that heat or microwave treatment changes both the grain shape and morphology of the sample. Large aggregates of ~20 μm crack into smaller fragments (5-10 μm) with a highly developed surface during processing. The evaporation of crystallization water causes the formation of micropores and microcracks and increases the surface area of the grains for further sorption of ammonium (NH_4^+) and phosphate (PO_4^{3-}) ions. Heat and microwave treatment of glauconite causes similar changes in the cation ratio.

Measurements of the BET surface area showed that high-temperature treatment leads to its reduction. However, it is important to note that this decrease is primarily attributed to the reduction in micropore surface area. Whereas the increase in the external surface area of the glauconite sample under the influence of microwave irradiation is accompanied by a decrease in the micro-pore area.

The best fit for the adsorption isotherm of both pollutants is given by Langmuir-Freundlich and BET models. The values of average free energy calculated from Dubinin-Radushkevich model were less than 8 kJ/mol, so the adsorption process is of a physical nature. The shapes of the phosphate and ammonia adsorption isotherms are quite different. The shape of PO_4^{3-} isotherm is of the type related to microporous materials, as opposed to the type of NH_4^+ isotherm where multi-layer adsorption occurs on a uniform non-porous surface. Therefore, it can be assumed that NH_4^+

is absorbed by the external surface of the samples, but phosphate ion is well fixed in the micropores. This coincides with the results of the porosity study of the samples before and after treatment. Moreover, it is the calcined sample that shows the lowest adsorption capacity for phosphate but the better adsorption capacity for ammonium. Conversely, for the microwave-irradiated sample, the adsorption capacity for phosphate increases, while that for ammonium remains at the same level.

The best result in phosphate uptake in dynamic conditions was shown by the natural glauconite and slightly worse by the microwave-irradiated sample. Thermal modification significantly worsens the sorption properties of glauconite for phosphate. A completely opposite phenomenon is observed in the ammonium absorption. The highest removal rate during the first hour is demonstrated by the natural and heat-treated samples. However, subsequently, the ammonium retention efficiency begins to decrease sharply for both the natural and microwave-irradiated samples. At the same time, the heat-treated sorbent continues effectively purifying water (more than 80% efficiency) even after 3 hours of exposure. Thus, in the case of ammonium nitrogen purification, heat treatment of glauconite significantly improves its sorption capacity. In general, all three columns removed ammonium nitrogen more efficiently than phosphate phosphorus.

Author Contributions: Conceptualization, K.S, I.F, A.M. and V.K.; methodology, K.S., A.M., V.K and D.P.; validation, K.S., I.F. and D.P.; formal analysis, K.S., I.F. and A.M.; investigation, K.S., I.F., A.M., V.K. and D.P.; resources, K.S., I.F., A.M. and V.K.; data curation, K.S., A.M. and D.P.; writing—original draft preparation, K.S., I.F., A.M., V.K. and D.P.; writing—review and editing, K.S., A.M., and D.P.; visualization, K.S., I.F., A.M., V.K and D.P.; supervision, K.S. and A.M. All authors have read and agreed to the published version of the manuscript.

Funding: This research was funded by Research Council of Lithuania and Ministry of Education and Science of Ukraine, according to the project “Sustainable technology of wastewater

treatment by environmentally friendly modified natural sorbents for removal of nitrogen, phosphorus and surfactants", financing agreement No. S-LU-22-1.

Conflicts of Interest: The authors declare no conflict of interest. The funders had no role in the design of the study; in the collection, analyses, or interpretation of data; in the writing of the manuscript; or in the decision to publish the results.

References

1. Barakan, S.; Aghazadeh, V. The advantages of clay mineral modification methods for enhancing adsorption efficiency in wastewater treatment: a review. *Environ. Sci. Pollut. Res.* **2021**, *28*, 2572–2599. https://doi.org/10.1007/s11356-020-10985-9.
2. Jones, E.R.; Bierkens, M.F.P.; Wanders, N. et al. Current wastewater treatment targets are insufficient to protect surface water quality. *Commun. Earth Environ.* **2022**, *3*, 221. https://doi.org/10.1038/s43247-022-00554-y
3. Mažeikienė, A.; Grubliauskas, R. Biotechnological wastewater treatment in small-scale wastewater treatment plants. *J. Clean. Prod.* **2021**, *279*, 123750. https://doi.org/10.1016/j.jclepro.2020.123750
4. Janicka, E.; Kanclerz, J.; Wiatrowska, K.; Budka, A. Variability of Nitrogen and Phosphorus Content and Their Forms in Waters of a River-Lake System. *Front. Environ. Sci.*, **2022**, *10*, 874754. https://doi.org/10.3389/fenvs.2022.874754
5. Wang, Q.; Liao, Z.; Yao, D.; Yang, Z.; Wu, Y.; Tang, C. Phosphorus immobilization in water and sediment using iron-based materials: a review. *Sci. Total Environ*. **2021**, *767*, 144246. https://doi.org/10.1016/j.scitotenv.2020.144246
6. Ding, S.; Sun, Q.; Chen, X.; Liu, Q.; Wang, D.; Lin, J.; Zhang, C.; Tsang, D.C.W. Synergistic adsorption of phosphorus by iron in lanthanum modified bentonite (Phoslock®): new insight into sediment phosphorus immobilization. *Water Res.* **2018,** *134*, 32–43. https://doi.org/10.1016/j.watres.2018.01.055

7. Han, H.; Rafiq, M.K.; Zhou, T.; Xu, R.; Mašek, O.; Li, X. A critical review of clay-based composites with enhanced adsorption performance for metal and organic pollutants. *J. Hazard. Mater.* ***2019,*** *369*, 780–796. https://doi.org/10.1016/j.jhazmat.2019.02.003
8. Ezzatahmadi, N.; Ayoko, G.A.; Millar, G.J.; Speight, R.; Yan, C.; Li, J.; Li, S.; Zhu, J.; Xi, Y. Clay-supported nanoscale zero-valent iron composite materials for the remediation of contaminated aqueous solutions: a review. *Chem. Eng. J.* **2017**, *312*, 336–350.
9. Stepova, K.; Fediv, I.; Mažeikienė, A.; Šarko, J.; Mažeika, J. Adsorption of ammonium ions and phosphates on natural and modified clinoptilolite: isotherm and breakthrough curve measurements. *Water* **2023**, *15*, 1933. https://doi.org/10.3390/w15101933
10. Xia, L.; David, T.; Verbeeck, M.; Bruneel, Y.; Smolders, E. Iron rich glauconite sand as an efficient phosphate immobilising agent in river sediments. *Sci. Total Environ.* **2022,** *811*, 152483. https://doi.org/10.1016/j.scitotenv.2021.152483
11. Vandermoere, S.; Ralaizafisoloarivony, N.A.; Van Ranst, E.; De Neve, S. Reducing phosphorus (P) losses from drained agricultural fields with iron coated sand (- glauconite) filters. *Water Res.* **2018**, *141*, 329-339. https://doi.org/10.1016/j.watres.2018.05.022.
12. Chauhan, M.; Saini, V.K.; Suthar, S. Enhancement in selective adsorption and removal efficiency of natural clay by intercalation of Zr-pillars into its layered nanostructure. *J. Clean. Prod.* **2020**, *258*, 120686. https://doi.org/10.1016/j.jclepro.2020.120686
13. Chang, Y.S.; Au, P.I.; Mubarak, N.M.; Khalid, M.; Jagadish, P.; Walvekar, R.; Abdullah, E.C. Adsorption of Cu(II) and Ni(II) ions from wastewater onto bentonite and bentonite/GO composite. *Environ Sci Pollut Res.* **2020**, *27(26)*, 33270-33296. https://doi.org/10.1007/s11356-020-09423-7

14. Turki, T., Frini-Srasra, N. & Srasra, E. Environmental Application of Acid Activated Kaolinite-Glauconite Clay Assisted by Microwave Irradiation. Silicon 14, 7939–7949 (2022). https://doi.org/10.1007/s12633-021-01531-4

15. Martemyanov, D.; Rudmin, M.; Zhuravkov, S.; Korotkova, E.; Godymchuk, A.; Haskelberg, M.; Martemyanova, I.; Chernova, A.; Tyabaev, A.; Artamonov, A.; Plotnikov, E. Application of ural glauconite for groundwater deironing and demanganation. *J. Environ. Sci. Health A.* **2021**, *56:8*, 861-866. https://doi.org/10.1080/10934529.2021.1932171

16. Georgescu, A-M.; Nardou, F.; Zichil, V.; Nistor, I.D. Adsorption of lead(II) ions from aqueous solutions onto Cr-pillared clays. *Appl. Clay Sci.* **2018**, *152*, 44–50. https://doi.org/10.1016/j.clay.2017.10.031

17. El Ouardi, M.; Laabd, M.; Abou Oualid, H.; Brahmi, Y.; Abaamrane, A.; Elouahli, A.; Ait Addi, A.; Laknifli, A. Efficient removal of p-nitrophenol from water using montmorillonite clay: insights into the adsorption mechanism, process optimization, and regeneration. *Environ. Sci. Pollut. Res. Int.* **2019,** *26(19),* 19615-19631. doi: 10.1007/s11356-019-05219-6

18. Bruneel, Y.; Van Laer, L.; Brassinnes, S.; Smolders, E. Radiocaesium sorption on natural glauconite sands is unexpectedly as strong as on Boom Clay. *Sci. Total Environ*. **2020**, *720*, 137392. https://doi.org/10.1016/j.scitotenv.2020.137392.

19. Pinelli, D.; Foglia, A.; Fatone, F.; Papa, E.; Maggetti, C.; Bovina, S.; Frascari, D. Ammonium recovery from municipal wastewater by ion exchange: Development and application of a procedure for sorbent selection. *J. Environ. Chem. Eng*. **2022**, *10 (6)*, 108829. https://doi.org/10.1016/j.jece.2022.108829

20. Guida, S.; Potter, C.; Jefferson, B. et al. Preparation and evaluation of zeolites for ammonium removal from municipal wastewater through ion exchange process. *Sci. Rep*. **2020,** *10*, 12426. https://doi.org/10.1038/s41598-020-69348-6.

21. Mucci, M.; Maliaka, V.; Noyma, N.P.; Marinho, M.M.; Lürling, M. Assessment of possible solid-phase phosphate sorbents to mitigate eutrophication: influence of pH and anoxia. *Sci. Total Environ.* **2018**, *619–620*, 1431–1440. https://doi.org/10.1016/j.scitotenv.2017.11.198

22. Vandermoere, S.; Ralaizafisoloarivony, N.A.; Van Ranst, E.; De Neve, S. Reducing phosphorus (P) losses from drained agricultural fields with iron coated sand (- glauconite) filters. *Water Res.* **2018**, *141*, 329-339. https://doi.org/10.1016/j.watres.2018.05.022

23. Rudmin, M.; Banerjee, S.; Makarov, B. Evaluation of the Effects of the Application of Glauconitic Fertilizer on Oat Development: A Two-Year Field-Based Investigation. *Agronomy* **2020**, *10*, 872. https://doi.org/10.3390/agronomy10060872

24. Martemianov, D.; Plotnikov, E.; Rudmin, M.; Tyabayev, A.; Artamonov, A.; Kundu, P. Studying Glauconite of the Bakchar Deposit (Western Siberia) as a Prospective Sorbent for Heavy Metals. J. *Environ. Sci. Health A* **2020**, *55*, 1359–1365. DOI: 10.1080/10934529.2020.1794686

25. Galangashi, M.A.; Kojidi, S.F.M.; Pendashteh, A.; Souraki, B.A.; Mirroshandel, A.A. Removing Iron, Manganese and Ammonium Ions from Water Using Greensand in Fluidized Bed Process. *J. Water Process. Eng.* **2021**, *39*, 101714. https://doi.org/10.1016/j.jwpe.2020.101714

26. Singla, R.; Alex, T.C.; Kumar, R. On mechanical activation of glauconite: Physico-chemical changes, alterations in cation exchange capacity and mechanisms, *Powder Technol*. ***2020***, *360*, 337-351, https://doi.org/10.1016/j.powtec.2019.10.035.

27. Cecilia, J.; García-Sancho, C.; Vilarrasa-García, E.; Jiménez-Jiménez, J.; Rodriguez-Castellón, E. Synthesis, characterization, uses and applications of porous clays heterostructures: a review. *Chem Rec* **2018,** *18*, 1085–1104.

28. Kotova, D.L.; Artamonova, M.N.; Krysanova, T.A. et al. The Effect of a Pulsed Magnetic Field on the Hydration Properties of Clinoptilolite and Glauconite. *Prot. Met. Phys. Chem. Surf.* **2018**, *54*, 598–602. https://doi.org/10.1134/S2070205118030073
29. Khabbouchi, M.; Hosni, K.; Mezni, M.; Srasra, E. Structural characterizations and mechanical behavior of activated clay-based $Si_5(PO_4)_6O$ and SiP_2O_7 compounds. *Silicon*. **2019**, *12 (8)*, 117-124. https://doi.org/10.1007/s12633-019-00218-1
30. Cherifi, Z.; Boukoussa, B.; Zaoui, A.; Belbachir, M.; Meghabar, R. Structural, morphological and thermal properties of nanocomposites poly(GMA)/clay prepared by ultrasound and in-situ polymerization. *Ultrason. Sonochem.* **2018**, *48*, 188–198. https://doi.org/10.1016/j.ultsonch.2018.05.027
31. Pozo-Rodríguez, M.; Pardo-Canales, L.; Essih, S.; Cecilia, J.A.; Dominguez-Maqueda, M.; Olmo-Sanchez, M.I.; Franco F. Modification of the textural properties of palygorskite through microwave assisted acid treatment. Influence of the octahedral sheet composition. *Appl Clay Sci.* **2020**, *196*, 105745. https://doi.org/10.1016/j.micromeso.2019.109749
32. Krol, M.; Rozek, P. The effect of calcination temperature on metakaolin structure for the synthesis of zeolites. *Clay Miner.* **2018**, *53*, 657-663. https://doi.org/10.1180/clm.2018.49.
33. Zhang, A.; Liu, J.; Yang, Y.; Yu, Y.; Wu, D. Experimental and theoretical studies on the adsorption performance of lead by thermal pre-activation and phosphate modified kaolin sorbent. *Chem. Eng. J.* **2023**, *451, Part 2*, 138762. https://doi.org/10.1016/j.cej.2022.138762
34. Zha J.; Huang, Y.; Clough,P.T.; Xia Z.; Zhu, Z.; Fan, C.; Yu, M.; Yan, Y.; Cheng, H. Green production of a novel sorbent from kaolin for capturing gaseous $PbCl_2$ in a furnace. *J. Hazard. Mater.* **2021**, *404, Part B*, 124045. https://doi.org/10.1016/j.jhazmat.2020.124045.

35. Sips, R. Combined form of Langmuir and Freundlich equations. *J. Chem. Phys.* **1948**, *16*, 490-495. https://doi.org/10.1063/1.1746922.
36. Dubinin, M.M. Physical Adsorption of Gases and Vapors in Micropores. In *Progress in Surface and Membrane Science;* Cadenhead, D.A., Danielli, J.F., Rosenberg, M.D., Eds.; Elsevier, 1975; Volume 9, pp. 1-70. https://doi.org/10.1016/B978-0-12-571809-7.50006-1.
37. Brunauer, S.; Emmett, P.H.; Teller, E. Adsorption of Gases in multimolecular layers. *J. Am. Chem. Soc.* **1938**, *60 (2)*, 309-319.
38. Stepova, K.; Sysa, L.; Konanets, R. Nonlinear Fitting of Iron Sorption on Bentonite to Theoretical Isotherm Models. *Phys. Chem. Solid State* **2022**, *23(2)*, 270-276. https://doi.org/10.15330/pcss.23.2.270-276.
39. Zhang, S.N.; Xiao, R.L.; Liu, F.; Wu, J.S. Interception effect of vegetated drainage ditch on nitrogen and phosphorus from drainage ditches. *Huanjing Kexue/Environ. Sci.* **2015**, *36*, 4516–4522. https://doi.org/10.13227/j.hjkx.2015.12.025.
40. Thommes, M.; Kaneko, K.; Neimark, A.V.; Olivier, J.P.; Rodriguez-Reinoso, F.; Rouquerol, J.; Sing, K.S.W. Physisorption of gases, with special reference to the evaluation of surface area and pore size distribution (IUPAC Technical Report). *Pure Appl. Chem.* **2015**, *87*, 1051–1069. https://doi.org/10.1515/pac-2014-1117.
41. Lambert, S.; Tran, K.Y.; Arrachart, G.; Noville, F.; Henrist, C.; Bied, C.; Moreau, J.J.E.; Wong Chi Man, M.; Heinrichs, B. Tailor-made morphologies for Pd/SiO_2 catalysts through sol–gel process with various silylated ligands. *Microporous Mesoporous Mater.* **2008**, *115*, 609–617. https://doi.org/10.1016/j.micromeso.2008.03.003.
42. Giles, C.H.; Smith, D.; Huitson, A. A general treatment and classification of the solute adsorption isotherm. I: Theoretical. *J. Colloid Interface Sci.* **1974**, *47*, 755–765. https://doi.org/10.1016/0021-9797(74)90252-5.

501 43. Sing, K.S.W.; Everett, D.H.; Haul, R.A.W.; Moscou, L.; Pierotti, R.A.; Rouquerol, J.;
502 Siemieniewska, T. Reporting physisorption data for gas-solid systems with special
503 reference to the determination of surface area and porosity. *Pure Appl. Chem.* **1985**, *57*,
504 603-619. https://doi.org/10.1351/pac198557040603.
505

Figure 1. Laboratory bench with three columns

Figure 2. SEM images of glauconite (SE detector on the left, BSE detector on the right): a - initial sample, b - calcined at 550 °C, c - microwave irradiated

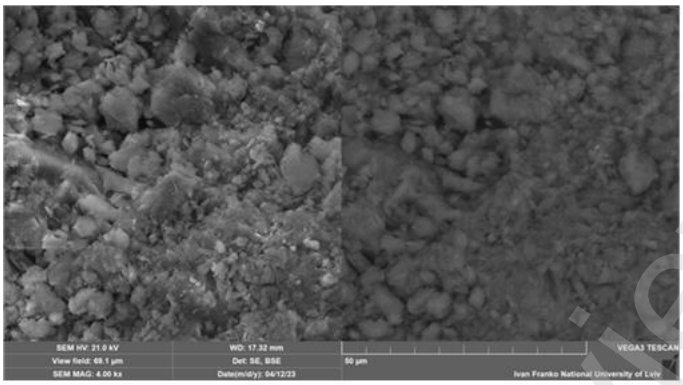

a

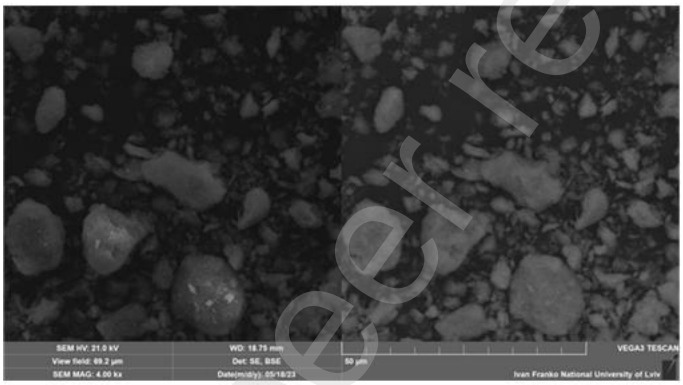

b

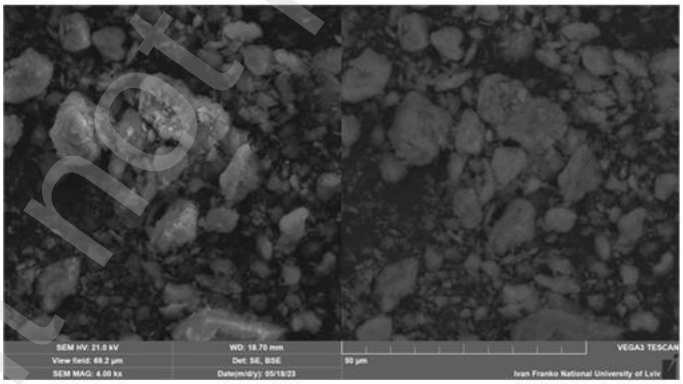

c

Figure 3. Elemental distribution on the surface of glauconite
a - initial sample, b - calcined at 550 °C, c - microwave irradiated

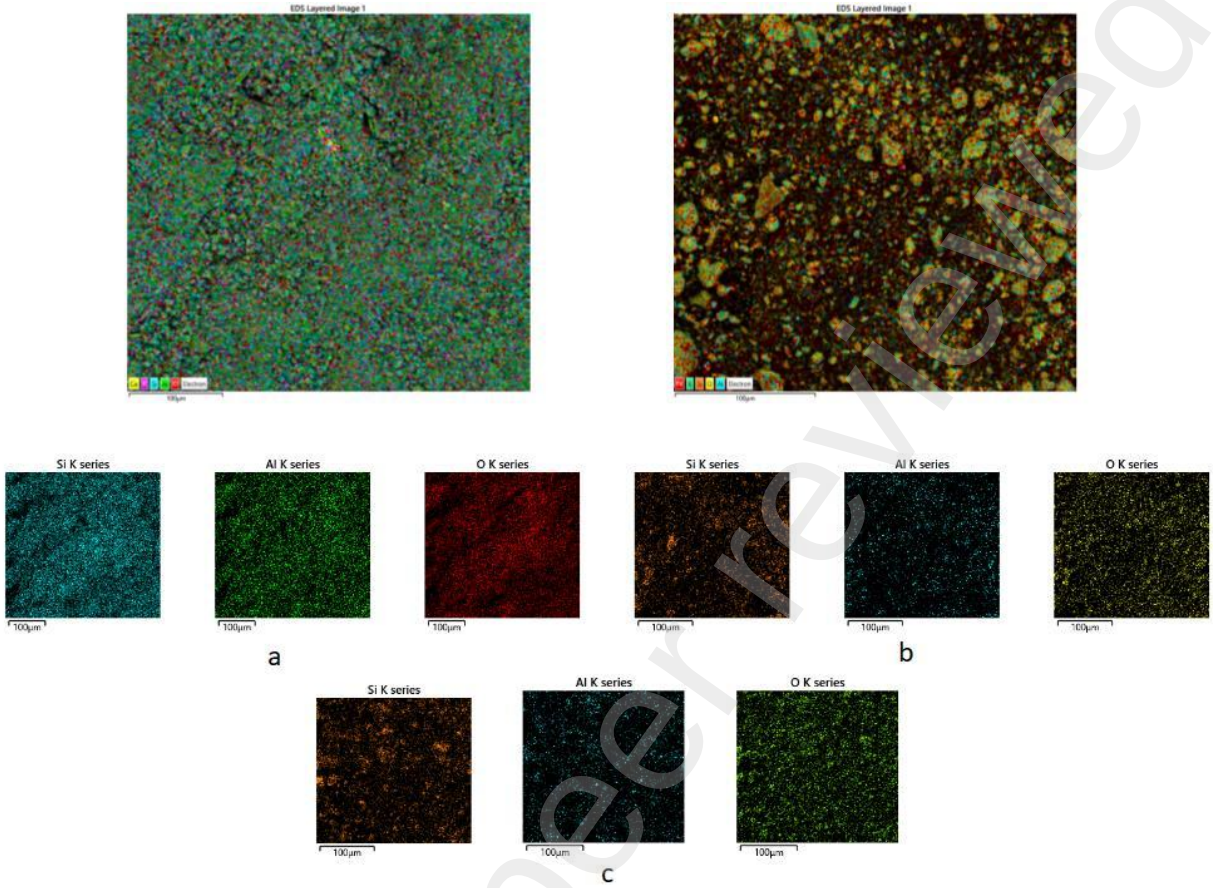

Figure 4. N_2 adsorption-desorption isotherms

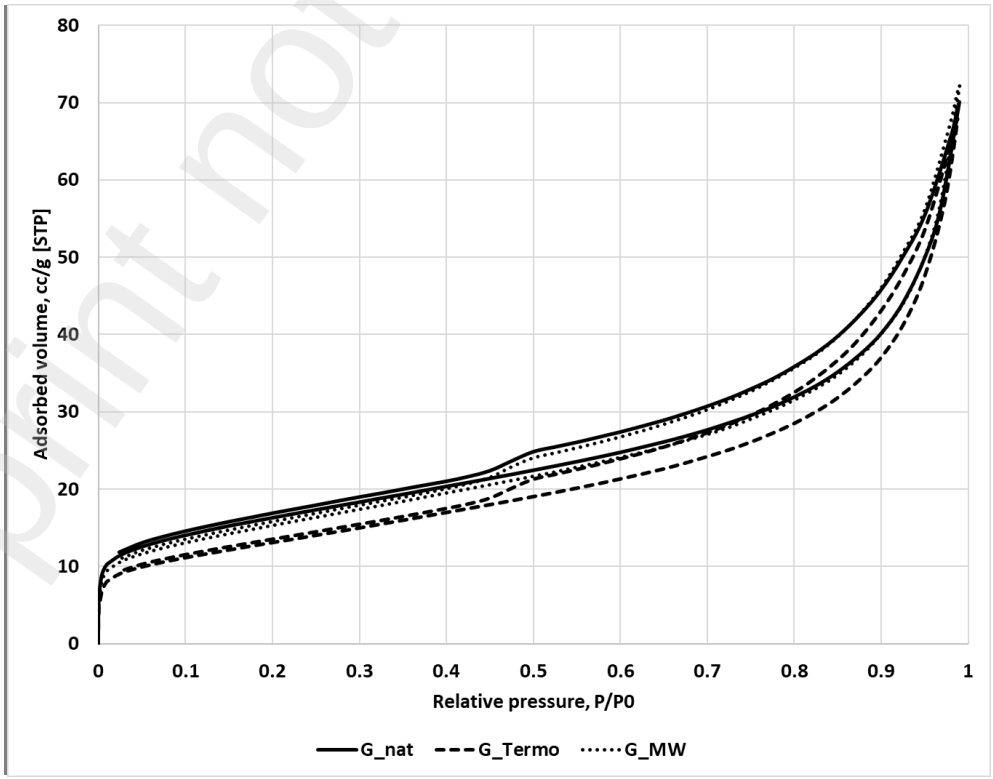

Figure 5. Pore size distribution

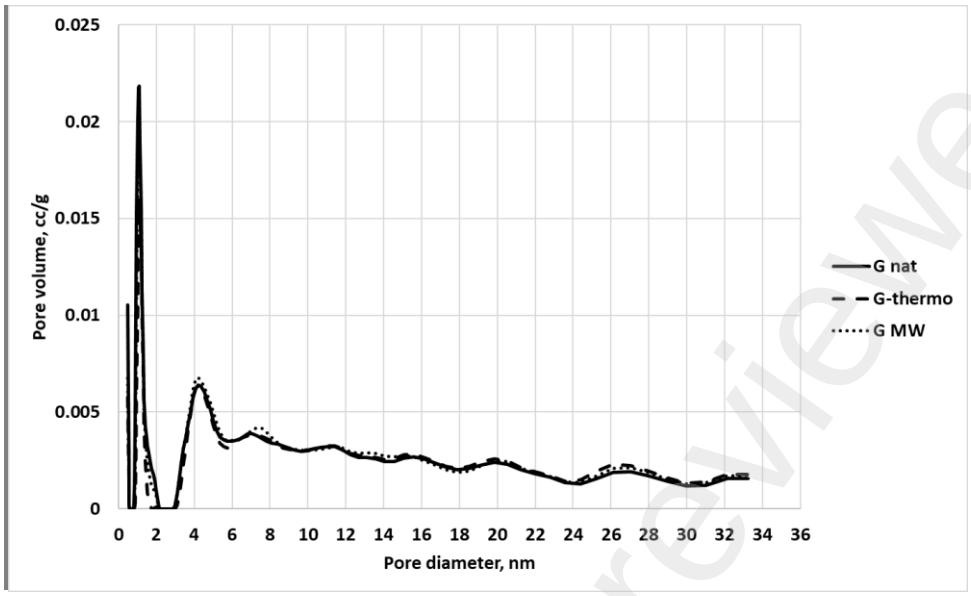

Figure 6. Isotherms of NH_4^+ adsorption

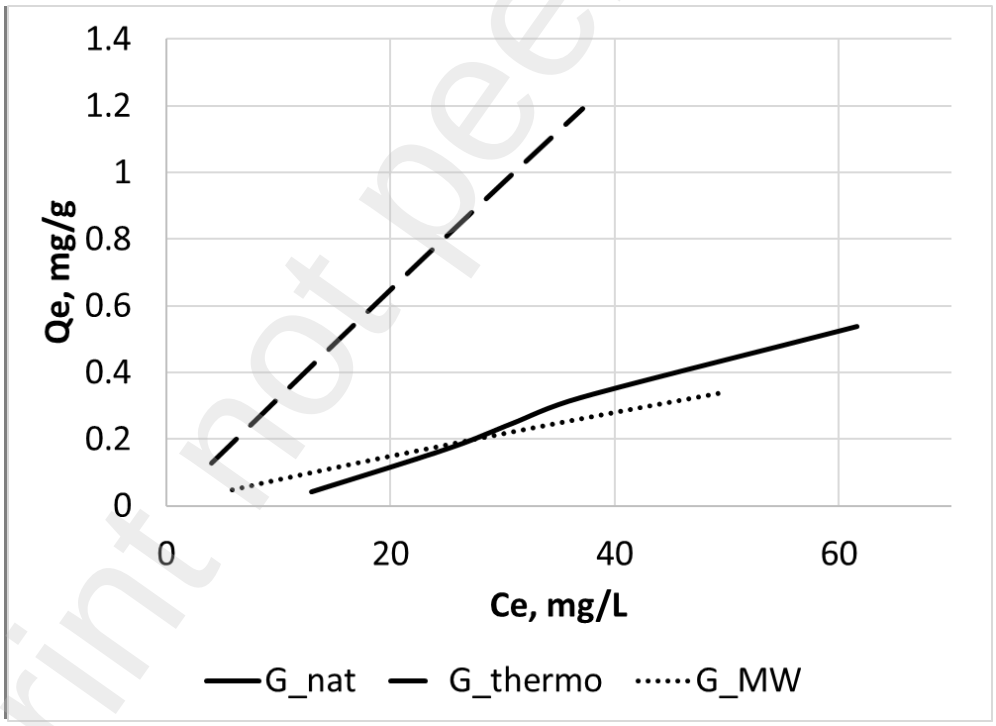

Figure 7. Isotherms of PO_4^{3-} adsorption

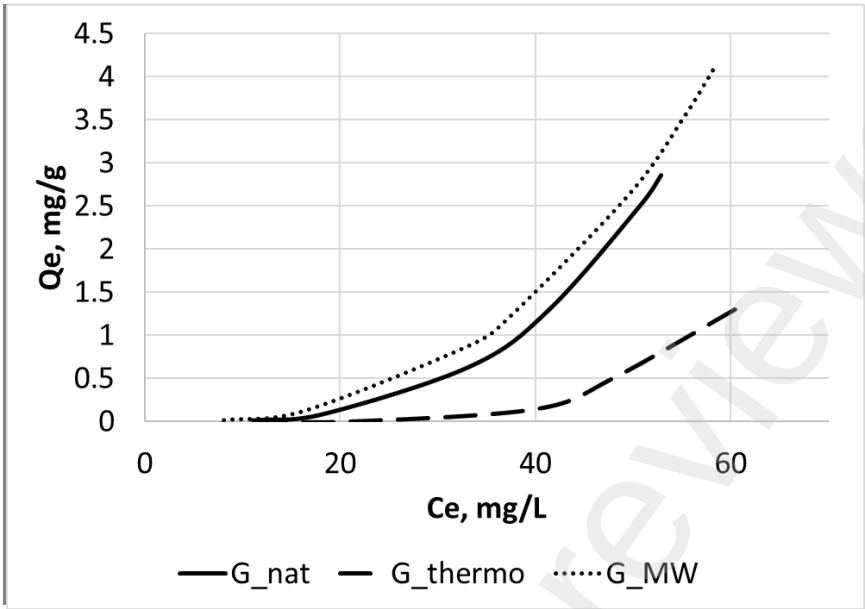

Figure 8. PO_4-P retention efficiency

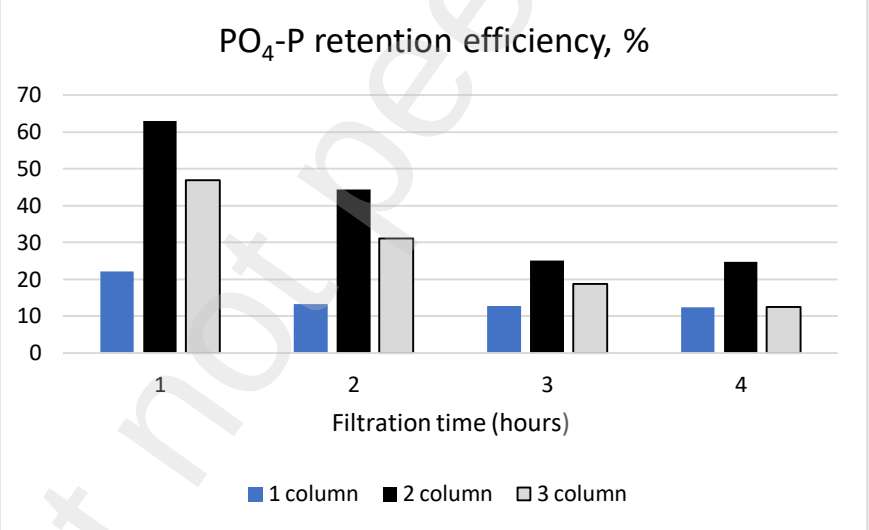

568 **Figure 9.** NH_4-N retention efficiency

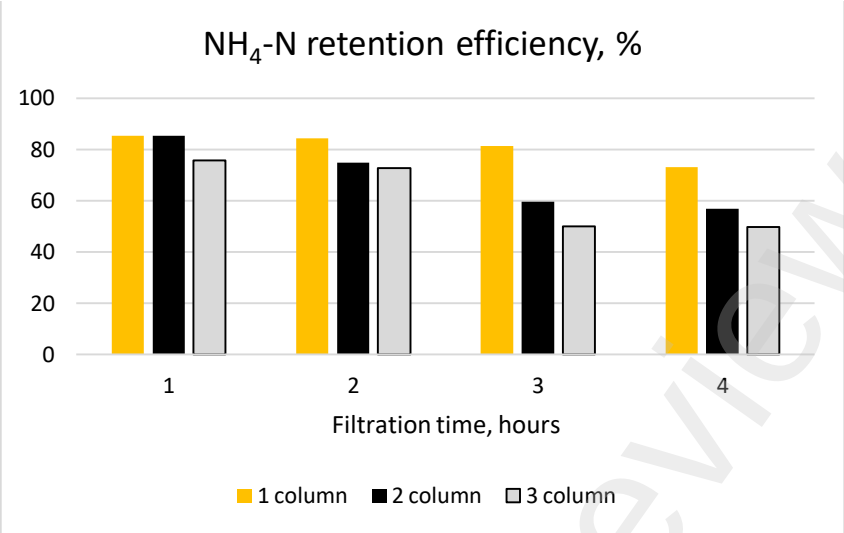

569
570
571

572 **Table 1.** Specific surface area (S_{BET}), micropore area (S_{mic}), external surface area (S_{ext}), pore
573 volume (V_p), equivalent particle size (d_{part}), and porosity (ε) of natural and modified clinoptilolite.

Sample code	S_{BET}, m^2/g	S_{mic}	S_{ext}	V_p, ml/g	d_{part}, nm	ε
G_nat	54.99	26.0	28.99	0.084	103.9	0.081
G_thermo	43.57	14.9	28.67	0.083	156,7	0.068
G_MW	50.28	20.1	30.18	0.086	107.3	0.087

574

575 **Table 2.** NH_4^+ adsorption isotherms nonlinear fitting parameters.

	Sample index		
	G_nat	**G_thermo**	**G_MW**
Langmuir-Feundlich isotherm			
q_m	0.723	20.67	4.37
K_{FL}	0.025	0.0018	0.0015
n_{FL}	2.503	1.027	0.96
SNE	3.65	4.1	3.54
R^2	1.0	1.0	1.0
Dubinin-Radushkevich isotherm			
q_m	4.286	4.695	1.052
β	0.041	0.021	0.021
SNE	23.03	26.01	23.64
R^2	0.97	0.97	0.94
BET isotherm			
q_m	0.0012	236.29	115.95
C_{BET}	1.07	0.28	0.84
SNE	6.20	5.68	4.85
R^2	0.93	0.99	0.97

576 **Table 3.** PO_4^{3-} adsorption isotherms nonlinear fitting parameters.

	Sample index		
	G_nat	**G_thermo**	**G_MW**
Langmuir-Feundlich isotherm			
q_m	113.58	1.78	101.21
K_{FL}	0.0062	0.0186	0.0055
n_{FL}	3.275	8.352	2.77
SNE	3.52	3.64	3.83
R^2	1.0	1.0	1.0
Dubinin-Radushkevich isotherm			
q_m	140	212.07	194.2
β	0.075	0.24	0.078
SNE	198.4	129.1	61.74
R^2	0.95	0.92	0.93
BET isotherm			
q_m	100.15	100.18	100.04
C_{BET}	0.01	0.0012	0.02
SNE	7.97	6.89	4.81
R^2	0.99	1.0	0.98

577